First-principles study of the $Co_2FeSi(001)$ surface and $Co_2FeSi/GaAs(001)$ interface

Sh. Khosravizadeh, S. Javad Hashemifar, and Hadi Akbarzadeh
Department of Physics, Isfahan University of Technology, 84156-83111 Isfahan, Iran
(Received 8 April 2009; published 4 June 2009)

Ab initio study of the electronic and magnetic properties of bulk Co_2FeSi, free $Co_2FeSi(001)$ surfaces, and its interfaces with GaAs(001) substrate are reported. The bulk computations indicate that the LSDA+U scheme is necessary to reproduce the measured total magnetic moments and to observe a half-metallic behavior. The thermodynamic stability of various $Co_2FeSi(001)$ surface and $Co_2FeSi/GaAs(001)$ interface terminations are studied in the framework of *ab initio* thermodynamics. The calculated surface phase diagram indicates that by tuning the atomic chemical potentials, three different terminations are probable. The obtained interface diagrams argue the possibility of the formation of mixed interfaces. The spin-polarized density of states shows that the half metallicity confirmed in the bulk Co_2FeSi is lost at its surfaces and interfaces with GaAs(001).

DOI: 10.1103/PhysRevB.79.235203 PACS number(s): 71.15.Mb, 75.70.Cn, 71.15.Dx

I. INTRODUCTION

Efficient spin injection from a ferromagnetic (FM) material into a semiconductor device, although has attracted considerable interests in recent years, is still far from being fully understood.[1] One of the main challenges in spin injection is the impedance mismatch that arises between the spin source and the semiconductor substrate during the diffusive transport process.[2] The most significant advantage of using half metals instead of an ordinary metallic ferromagnet as a spin source is their ability to circumvent this obstacle and obtain efficient spin injection. Half-metallic ferromagnets have metallic behavior in one spin channel and semiconductor behavior in the other, leading to an integer number of total spin moment. So, in principle, a 100% spin polarization at the Fermi level is expected for these materials. A point worth noticing is that even if a material has half-metallic character at the bulk regime, there is no guarantee to save such behavior in the surface and interface areas; a nonmagnetic (NM) layer at the interface or even a dilute disorder around this area may significantly reduce the spin polarization at the Fermi level.[3,4]

The Co-based full Heusler alloys due to their half-metallic behavior, high magnetic moment, and Curie temperature have attracted much attention.[5,6] Recently, Wurmehl *et al.*[7,8] experimentally and computationally investigated the structural, electronic, and magnetic properties of the bulk Co_2FeSi and showed that this alloy has the highest magnetic moment and Curie temperature among all studied half-metallic ferromagnets. These two quantities are of great importance for magnetic materials to be used in magnetic devices. Furthermore, huge magneto-optical effects have also been reported in this alloy.[9,10]

By inspecting the spin-resolved density of states (DOS) of Co_2FeSi, it has been revealed that the half-metallicity and magnetic properties of this alloy are very sensitive to the Fermi energy position.[7] This sensitivity roots in the fact that the Fermi level in the spin-down channel is located around the threshold of the conduction band and, hence, a small deviation in its position can cause significant changes in electronic and magnetic properties of this material. By investigating the dependence of the electronic structure on the lattice parameter of Co_2FeSi, Kandpal *et al.*[11] concluded that local spin-density approximation (LSDA) and generalized gradient approximation (GGA) are not sufficient for explaining the accurate properties of this alloy. They improved their calculations by considering the on-site correlation within LDA+U and concluded that moderate effective Coulomb exchange-correlation energies of around 2–5 eV lead to half-metallic ferromagnetism and measured integer magnetic moment at the experimental lattice parameter.

Co_2FeSi has a cubic L21 structure consisting of four interpenetrating fcc sublattices with a lattice parameter almost equal to the corresponding value reported for GaAs. The ignorable lattice mismatch and the structural similarity between the two compounds have made GaAs an appropriate substrate to grow Co_2FeSi layers. Hashimoto *et al.*[12,13] recently grew Co_2FeSi thin films on GaAs(001) substrate by molecular-beam epitaxy and studied the thermal stability at the interface. They showed that Co_2FeSi films are thermally much more stable than conventional ferromagnetic metals on GaAs and hence are more promising candidates for the efficient spin injection into semiconductors. The spin polarization (P) and tunneling magnetoresistance (TMR) of epitaxially grown Co_2FeSi thin films on a MgO(001) substrate were measured by Gercsi *et al.*[14] The measured P value of the ordered film was about 0.49 and the values obtained for TMR at 5 and 298 K were 67.5% and 43.6%, respectively. These TMR values were also confirmed in Ref. 15.

Although the electronic and magnetic properties of bulk Co_2FeSi have been extensively studied and additionally several groups have experimentally grown Co_2FeSi on GaAs substrate, to the best of our knowledge, no theoretical *ab initio* study of the Co_2FeSi free surfaces and its interfaces with GaAs have appeared in the literature. Hence, we found it useful to employ density-functional theory (DFT) calculations to study the electronic and magnetic properties of $Co_2FeSi(001)$ free surface and $Co_2FeSi/GaAs(001)$ interface. In the following, we first explain our computational method. Then, the bulk structure is optimized by first using GGA and then adding LDA+U correction to improve the electronic and magnetic results. U parameter was obtained by adjusting the bulk magnetic moment with the measured value. The surface and interface results are discussed in two

TABLE I. The calculated bulk properties of Co_2FeSi and four other Heusler alloys within GGA. a(Bohr): lattice parameter; B(GPa): bulk module; $M(\mu_B)$: total magnetic moment per formula unit; and E_C(Ry): cohesive energy per formula unit. NM, FM, and expt indices stand for nonmagnetic state, ferromagnetic state, and experimental value, respectively. The column "Ref." indicates the references of the calculated data. TW stands for "this work."

Co_2XSi	Ref.	a_{FM}	a_{NM}	B_{FM}	B_{NM}	a_{expt}	Ref.	M	M_{expt}	Ref.	E_C (FM)	E_C (NM)	T_C	Ref.
Co_2FeSi	TW	10.65	10.47	203	240	10.66	16	5.70	6.00	7	−1.66	−1.55	1100	7
$Co_2Cr_{0.5}Fe_{0.5}Al$ [a]	17	10.75	10.66	187	201	10.83	18	3.99	3.65	19			665	20
Co_2MnSi	21	10.64	10.51	221	238	10.68	22	5.00	5.00	23	−1.51	−1.38	985	23
Co_2FeAs	TW	10.95	10.69	160	212			6.08			−1.38	−1.28		
Co_2FeGa	TW	10.81	10.68	186	213	10.84	24	5.06	5.03	25	−1.65	−1.51	1093	26

[a]The corresponding experimental data have been measured for $Co_2Cr_{0.6}Fe_{0.4}Al$ alloy.

separate subsections and the summary of the results is presented in the last section.

II. COMPUTATIONAL APPROACH

All of our calculations are based on the spin-polarized density-functional theory. To optimize bulk, surface, and interface structures and to calculate their structural properties, we used the highly efficient computer program PWSCF that is a pseudo-potential-plane-wave (PP-PW) code. The exchange-correlation term was approximated by the GGA in the form proposed by Perdew, Burke, and Ernzerhof (PBE).[27] For this part of calculation, ultrasoft pseudopotentials were used and the valence electronic wave functions were expanded by a plane-wave basis set with a kinetic-energy cutoff of 40 Ry. The Methfessel-Paxton[28] smearing method with broadening parameter of 0.02 Ry was used.

As the bulk magnetic properties of this alloy within GGA are somewhat different from the measured data, we performed a more accurate electronic calculation by using GGA+U within WIEN2K, an all electron full potential augmented plane-wave code. In this part of calculations, the atomic sphere radii of Co, Fe, Si, Ga, and As were set to 2.29, 2.29, 2.15, 2.19, and 2.27 bohr, respectively. The charge density was Fourier expanded up to $G_{max}=12$ $Ry^{1/2}$. The maximum angular quantum number for the expansion of wave functions inside the atomic spheres was $l_{max}=10$ and the cutoff of the plane-wave expansion in the interstitial region (outside atomic spheres) was set to $K_{max}=7/RMT$, where RMT is the smallest atomic sphere in the system. The surface and interface structures were simulated by using the supercell approach with a regular k-point mesh according to Monkhorst-Pack[29] scheme.

III. BULK PROPERTIES

Since the bulk calculations of Co_2FeSi have already been reported by others,[7,8] we focus on those features of the bulk properties that have not been touched by others. First of all, we optimized the bulk structural parameters within GGA and then the electronic structure and magnetic moments were calculated by using these optimized parameters. The obtained bulk properties of this alloy in comparison to four other Heusler alloys which have already been studied in our group are represented in Table I. In accordance with other reports, the GGA calculated magnetic moment per formula unit ($5.7\mu_B$) is lower than the experimental value ($6\mu_B$) and DOS graph does not confirm the half metallicity (Fig. 2). Hence, for better description of the electronic structure and magnetic moment of Co_2FeSi, we followed Kandpal *et al.*[11] and applied the GGA+U scheme to our calculations to enhance the on-site electron correlation. Due to the good agreement with experiment, the GGA lattice constant was adopted for GGA+U investigations and the electronic structure of the system was calculated at several values of effective U parameter. Variation in the total magnetic moment as a function of U is plotted in Fig. 1 and the obtained d partial DOS (PDOS) at four selected values of U is presented in Fig. 2.

We observe that the magnetic moment increases by increasing U parameter from 0 to about 2 eV and then is fixed at the experimental value of $6\mu_B$ in the range of $U=2-5.5$ eV. Therefore, in this range of effective Coulomb exchange interaction (2–5.5 eV), GGA+U predicts a half-metallic character for Co_2FeSi, in agreement with Kandpal *et al.*[11] Considering partial DOS plots (Fig. 2), as expected, we observe that by increasing U the minority conduction states move toward higher energies; this shift is more clearly visible in the Fe, e.g., orbital which occupies the lowest conduction states within GGA parametrization, and half-metallic gap originates from their shift away from the Fermi level. Although the shifts of the minority partial DOS in the range of $U=0-2$ eV have minor effects on the total number of d electrons, they cause an on-site charge transfer from minority to majority orbitals both for Co and Fe ions. In the range of $U=2-5.5$ eV, the Fermi energy is inside the half-metallic gap and hence the orbital occupations numbers—and accordingly magnetic moments—remain constant.

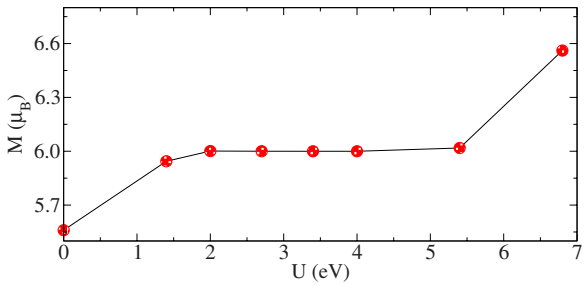

FIG. 1. (Color online) Variation in the total magnetic moment M per formula unit as a function of effective U parameter.

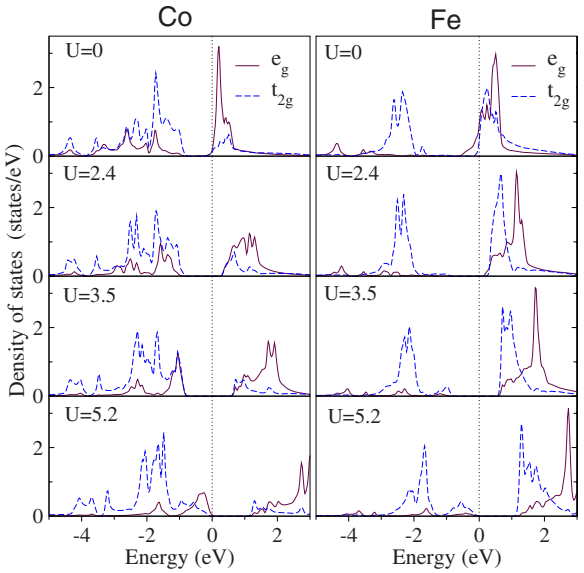

FIG. 2. (Color online) The minority *eg* (solid line) and t_{2g} (dashed line) partial DOS of Co (left column) and Fe atoms (right column) within four different values of *U* parameter. Values of *U* given in the plots are in eV and $U=0$ stands for standard PBE-GGA calculation.

Although all values of *U* between about 2 and 5.5 eV give rise to a total magnetic moment of $6\mu_B$ in full agreement with experimental result, applying the larger values in this interval leads to large changes in the electronic structure (Fig. 2), and this large modification in GGA needs strong arguments. Therefore, we selected smaller values of this interval ($U_{Co}=2.6$ eV, $U_{Fe}=2.5$ eV) which are sufficient to produce measured magnetic moment and, moreover, are consistent with the first-principles Hartree-Fock-calculated values of effective *U* parameter (taking into account screening effects) for transition-metal elements.[30]

A more detailed investigation of the partial DOS of majority-spin channel (not shown in Fig. 2) indicates that almost all of the *d* orbitals are occupied. By increasing *U* in GGA+*U*, these occupied states shift away from the Fermi level toward lower energies. In the minority-spin channel, it is clearly seen that the highest valence states originate from Co t_{2g} orbitals, while the lowest conduction states are mainly Fe *eg* orbitals. Other *d* orbitals of Co and Fe atoms have also some rather small contributions to the low-energy conduction states beginning from slightly below the Fermi level. These results indicate that Co_2FeSi does not follow Galanakis *et al.* explanation about Co_2MnZ alloys that the minority gap is controlled and surrounded by Co *eu* and Co *t*1*u* orbitals.[31] The Fe *eg* orbital in the minority band of Co_2FeSi, unlike the almost empty minority Mn *eg* orbital of Co_2MnZ, is partially occupied; hence its energy level is rather lower than the corresponding Mn state. Consequently, the antibonding *d* orbitals due to the coupling of Fe *eg* and CoCo *eg* orbitals in Co_2FeSi have lower energy with respect to nonbonding *eu* orbitals originated from two Co atoms.

In order to verify this idea, we calculated and compared the minority band-edge character of some other similar full Heusler Co_2YSi alloys (*Y*=Ti, V, and Cr). It was found out that in all of these three compounds, similar to Co_2MnSi and consistent with the Galanakis model, the half-metallic gap is only surrounded by Co orbitals. This observation is attributed to the fact that the spin down *eg* orbitals of Ti, V, and Cr similar to Mn are empty. Therefore, we conclude that in the full Heusler Co_2YZ alloy, the minority band-edge characters are substantially affected by the minority Y *eg* orbital. If this orbital is empty then the half-metallic gap is controlled by Co *d* orbitals; otherwise, Y *d* orbitals will also contribute to the states around the half-metallic gap.

IV. SURFACE PROPERTIES

Co_2FeSi with L21 lattice structure has four atomic layers per conventional cubic unit cell in (001) direction that are Co, FeSi, Co, and SiFe layers. The Co layers are equivalent and composed of 2 Co atoms per unit cell; hence, we call them CoCo layers in this paper. Since the FeSi and SiFe layers are also symmetrically equivalent then there are only two possible ideal terminations along (001) direction: CoCo and FeSi. In view of other similar studies that have been done in our group on the surface and interface of some Co_2XY-based full Heusler alloys (Co_2MnSi, $Co_2Cr_{0.5}Fe_{0.5}Al$), it has been shown that a modified artificial termination consisting of pure *X* element can change the half metallicity significantly.[17,21] Hence, the modified FeFe termination was also considered and we studied three distinct terminations. This Fe rich surface is created by substituting the Si atom with Fe in the FeSi terminations.

In order to calculate the surface properties of Co_2FeSi, we used 1×1 supercells containing some atomic layers stacked along (001) direction with vacuum regions assumed on both sides of the slabs. The slabs were thick enough to reproduce the bulklike properties at the central layers. Furthermore, the thickness of the vacuum region is assumed large enough to avoid the interaction of adjacent slabs. We verified that a slab of 13 atomic layers and a 20 bohr vacuum region fulfill these criteria. In order to prevent the creation of the surface dipole, symmetrical slabs with two identical surface terminations were used in our computations. After relaxing the atomic positions to reduce the forces acting on them down to 1 mRy/bohr, the total energy per unit cell for all three surfaces was calculated.

In order to study the relative stability of different terminations, we compared their surface free energy as a function of atomic chemical potentials within the framework of *ab initio* atomistic thermodynamics.[32] The surface free energy is defined as

$$\gamma = \frac{1}{2A}\left[G - \sum_i (\mu_i N_i)\right]. \quad (1)$$

Where N_i and μ_i are the number and chemical potential of the *i*th atom, *G* is the Gibbs free energy of the slab, 2*A* is the total surface area of the supercell, and γ is the surface free energy per unit of the surface area. Following other studies,[33] it is reasonable to ignore the dynamical contributions to the Gibbs free energy at sufficiently low temperatures and only use DFT-calculated total energy to obtain the surface free

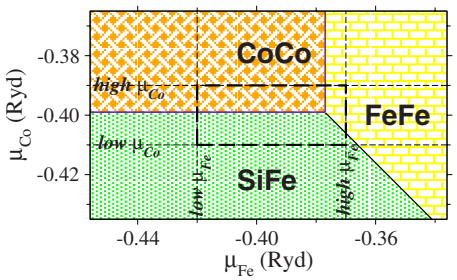

FIG. 3. (Color online) The calculated phase diagram of the $Co_2FeSi(001)$ surface terminations. The shadings show the regions of stability of various terminations, thin dashed lines mark the low and high limits of the chemical potentials, and the thick dashed line indicates the thermodynamically accessible region of the phase diagram.

energy. In order to obtain the phase diagram, we have to compare the surface free energies of different terminations in a reasonable range of chemical potentials to find the stable surface with the lowest surface free energy for any given values of chemical potentials. A noticeable point in plotting the phase diagram is that although we have three elements in this alloy, their corresponding chemical potentials are not independent. Since the surface of the slab is assumed to be in thermodynamic equilibrium with its central bulk layers then the appropriate equilibrium condition can be written as

$$2\mu_{Co} + \mu_{Fe} + \mu_{Si} = g_b, \tag{2}$$

where g_b is the Gibbs free energy of the bulk Co_2FeSi. By substituting μ_{Si} from this expression into Eq. (1), the relation of the surface free energy versus μ_{Co} and μ_{Fe} is obtained. It is clear that very high values of μ_{Co} (μ_{Fe}) arise the cobalt (iron) bulk structure, so the allowed region of the phase diagram is limited by the Gibbs free energies of bulk cobalt and iron. Hence, the higher limits of μ_{Co} and μ_{Fe} are corresponding to

$$\mu_{Co} = g_{Co}, \mu_{Fe} = g_{Fe}. \tag{3}$$

On the other hand, by decreasing μ_{Co} (μ_{Fe}), the Co (Fe) atoms leave the structure and FeSi (Co_2Si) structure will form; so the allowed region is restricted to the lower limits of μ_{Co} and μ_{Fe} as follows:

$$\mu_{Co} = 1/2(g_b - g_{FeSi}),$$

$$\mu_{Fe} = (g_b - g_{Co_2Si}). \tag{4}$$

Figure 3 shows the calculated phase diagram of the various investigated surfaces; the label on each region denotes the termination with the lowest surface free energy. According to this diagram, by tuning the chemical potentials within their allowed ranges all three terminations are accessible. Furthermore, it is clearly seen that by increasing μ_{Co}, the CoCo termination is more favorable while by increasing μ_{Fe}, the Fe rich surface is the stable one.

Our previous first-principles investigations on (001) surfaces of Co_2MnSi and $Co_2Cr_{0.5}Fe_{0.5}Al$ Heusler alloys indicate the instability of CoCo terminations in these systems, while in the present work we realized the stability of this termination in Co_2FeSi Heusler alloy. In order to understand the origin of this difference, we calculated the $Co_2CrSi(001)$ surfaces and found that similar to Co_2MnSi, the CoCo termination of this alloy is less stable than CrSi. In Table II, we have compared the computed parameters of these three Co-based Heusler alloys. We use the atomic cohesive energies calculated and listed in Table II to explain the different behaviors of Co_2FeSi. Since the cohesive energy is a qualitative measure of bonding desirability, atoms with lower cohesive energy are expected to be less stable at the surfaces. This is in agreement with the observed behavior of these three Heusler alloys. The cohesive energy of Co atom is substantially lower than Mn and Cr atoms. Hence, MnSi and CrSi terminations are expected to be more stable than CoCo termination in Co_2MnSi and Co_2CrSi alloys, respectively. In contrast, Fe and Co atoms have comparable cohesive energies leading to the comparable stability of these two terminations in Co_2FeSi Heusler alloy.

In order to study the electronic structure of different terminations, we calculated the PDOS of all three accessible surfaces within GGA and GGA+U approaches (Fig. 4). The calculated atomic magnetic moments of surface and subsurface Fe and Co atoms are also listed in Table III along with the bulk magnetic moments for comparison. By comparing the results of two approximations, it is generally observed that the on-site correlation imposed by GGA+U causes rather sharper Fe states around the Fermi level. It is clearly seen that the surface Fe atoms in the SiFe and FeFe terminations do not contribute to the spin-up DOS at the Fermi level, as a result of which they only enhance the negative spin polarization at the Fermi level. The subsurface Co atoms do not change this trend significantly. This means that the SiFe and FeFe surfaces of Co_2FeSi have a very high negative spin polarization, while in a couple of layers below surface (near bulk regime) there is an almost complete positive spin polarization at the Fermi level.

TABLE II. The calculated (001) surface energies of three full Heusler alloys along with some useful bulk cohesive energies, $E_C(X)$ and E_C (Heusler) (Ry): the cohesive energy of bulk X and bulk Co_2XSi alloy, E_S(CoCo) and $E_S(X\text{Si})$ (Ry): the surface energy of CoCo(001) and XSi(001) terminations, and $M(\mu_B)$: the total bulk magnetic moment per formula unit.

Co_2XSi	Xd shell	E_C (X)	E_C (Si)	E_C (Co)	E_C (Heusler)	E_S (CoCo)	E_S (XSi)	M (bulk)
Co_2CrSi	$3d^4$	−0.28	−0.36	−0.39	−1.54	0.39	0.33	3.0
Co_2MnSi	$3d^5$	−0.29	−0.36	−0.39	−1.51	0.60	0.17	5.0
Co_2FeSi	$3d^6$	−0.37	−0.36	−0.39	−1.67	0.38	0.44	6.0

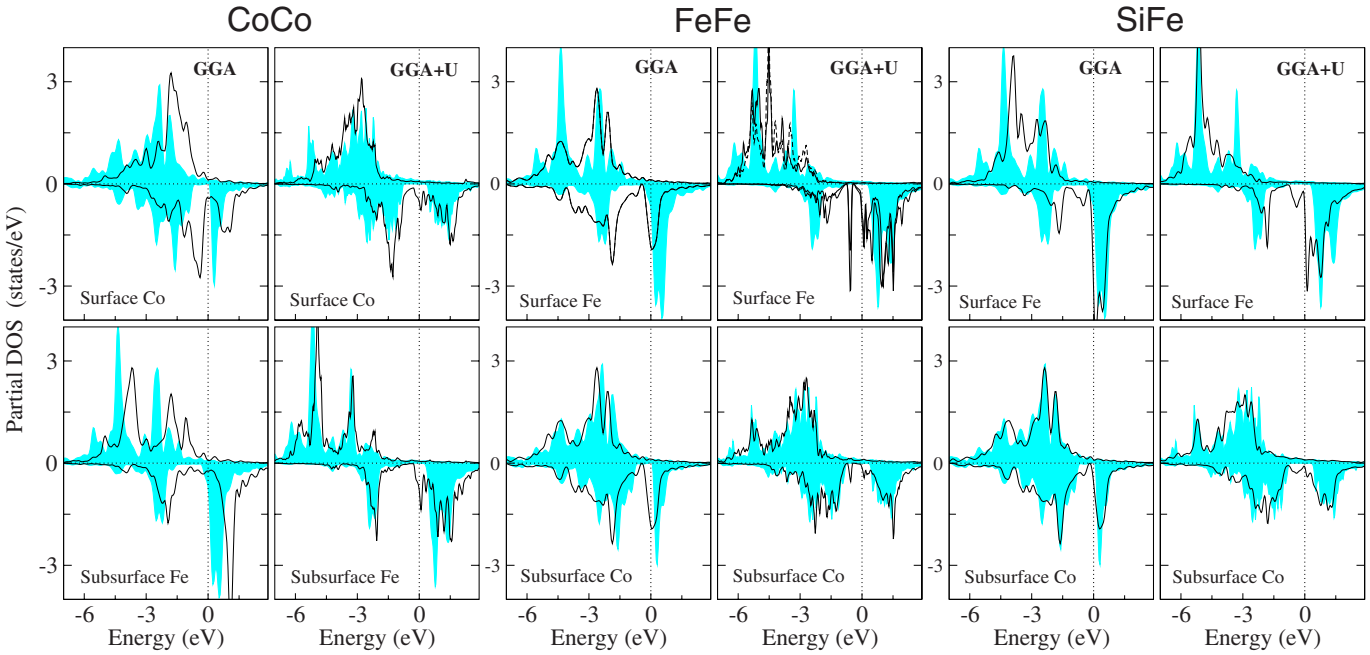

FIG. 4. (Color online) The *d* partial DOS of the surface and subsurface Fe and Co atoms at the stable SiFe, FeFe, and CoCo surface terminations within GGA and GGA+*U*. The shaded areas are corresponding bulk DOS. The Fermi energy is set to zero.

The reduction in the atomic coordination numbers at surfaces may arise various surface effects. Reducing the number of neighboring atoms weakens the crystal field consequently, enhancing exchange interactions at the surface atoms. Therefore, the calculated atomic magnetic moments (Table III) are larger at the surfaces compared with the bulk values. Another consequence of the crystal-field weakening is decreasing the bonding-antibonding splitting at surfaces, obviously visible in the minority channels of surface atoms at all studied terminations (Fig. 4). As a result of that, in the SiFe termination the lower part of the minority conduction surface states, which are mainly Fe *d* orbitals, moves toward lower energies and penetrates below the Fermi level. Therefore, at the SiFe surface, the Fe atoms are responsible for destroying the half metallicity observed for the bulk material within GGA+*U*. Increasing Fe concentration at the surface by replacing Si atom with Fe can only create more localized surface states and subsequently higher negative spin polarization at the Fermi level.

In the case of the CoCo termination within GGA, Co t_{2g} orbitals, which mainly determine lower-energy limit of the minority-spin gap, shift to higher energies and fill up the half-metallic gap. This is another effect that may happen at surfaces and originates from the surface potential. The bulk negative electrostatic potential should rise at surfaces to match to the vacuum zero potential level. This behavior may apply an overall shift in DOS toward higher energies, visible in the surface and subsurface atomic PDOS of CoCo termination obtained within GGA. It is observed that applying GGA+*U* diminishes the effect of the surface potential at the CoCo termination and shifts DOS toward lower energies. A point worth mentioning is that within GGA, the local PDOS and magnetic moment of the subsurface atoms indicate that when Co atoms are at the surface, the subsurface atoms are more affected by the surface potential.

Next we investigated relaxed atomic positions at the surfaces. The schematic representation of atomic displacements with respect to the ideal positions is illustrated in Fig. 5. In the SiFe termination, it is evidently seen that the surface Si atom tends to be closer to the slab, while Fe atoms move away from the bulk region. This behavior of Fe atoms is held in the FeFe termination where one of the surface Fe atoms get far from the subsurface Co layer. Because of nonequivalent positions of the surface Fe atoms in this termination, these two atoms undergo different displacement with respect to the nonrelax positions, and this yields a value of 0.07 bohr

TABLE III. The surface and subsurface atomic magnetic moments (in μ_B) at the $Co_2FeSi(001)$ stable surface terminations. The surface values are bold to be more recognizable. The bulk values are given for comparison.

	Bulk		SiFe		FeFe		CoCo	
	GGA	GGA+*U*	GGA	GGA+*U*	GGA	GGA+*U*	GGA	GGA+*U*
Co	1.29	1.51	1.25	1.56	1.43	1.71	**1.34**	**1.95**
Fe	3.06	3.16	**3.23**	**3.37**	**3.14,3.24**	**3.35,3.29**	**2.84**	3.15

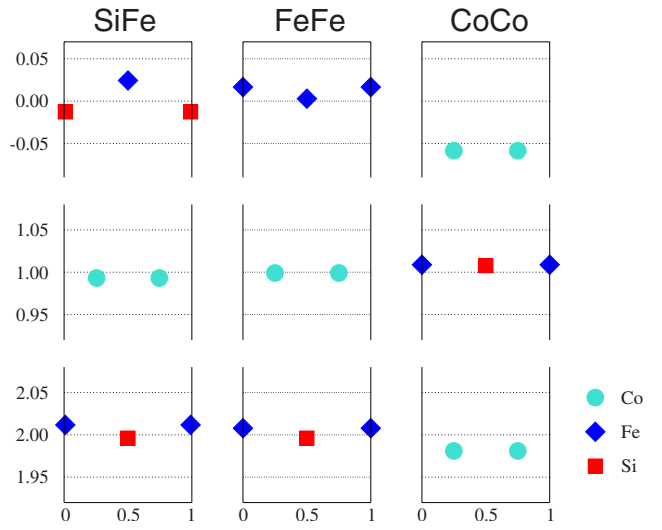

FIG. 5. (Color online) Schematic representation of the relaxed atomic positions at the $Co_2FeSi(001)$ surfaces. Vertical axis shows the z component of positions in units of interlayer distance. The values of $z=0$, $z=1$, and $z=2$ indicate nonrelax positions of the surface, subsurface, and next to the subsurface layers. Vertical movement of atoms from ideal nonrelax positions are magnified to be more visible.

roughness at this surface. In contrast, two Co atoms at the CoCo surface move identically inward the slab, so the zero value of roughness follows. Through detailed comparison of the atomic positions at different terminations, we can qualitatively state that Co-Si bonding is more favorable than Co-Fe. In order to verify this statement, we tried to estimate the relative bonding energies. Noting the fact that Co_2FeSi can be considered as Co_2Fe and Si or Co_2Si and Fe sublattices, we evaluated bonding energies by calculating the difference between the sum of energies of corresponding sublattices and the energy of Co_2FeSi structure. According to this approach, we obtained E_{bond}(Co-Fe)=−2.03 eV and E_{bond}(Co-Si)=−2.19 eV, in agreement with our previous conclusion.

V. INTERFACE RESULTS

Next, we studied the structural, electronic, and magnetic properties of $Co_2FeSi/GaAs(001)$ interface. To do that, we used supercells containing some atomic layers of the alloy in contact with some atomic layers of the semiconductor. In order to form an epitaxial interface, the in-plane lattice parameters of the alloy were set to the lattice parameter of GaAs and perpendicular lattice constant was optimized by minimizing the total energy per unit cell. The number of atomic layers of two materials is large enough so that atoms at the central layers show bulklike behaviors, and the distance between two slabs (of two materials) was optimized to minimize the stress and the energy.

Depending on which terminations of two materials are selected, there exist different possibilities. We considered all four possible ideal interface terminations in (001) direction, including CoCo and SiFe terminations in the Heusler alloy

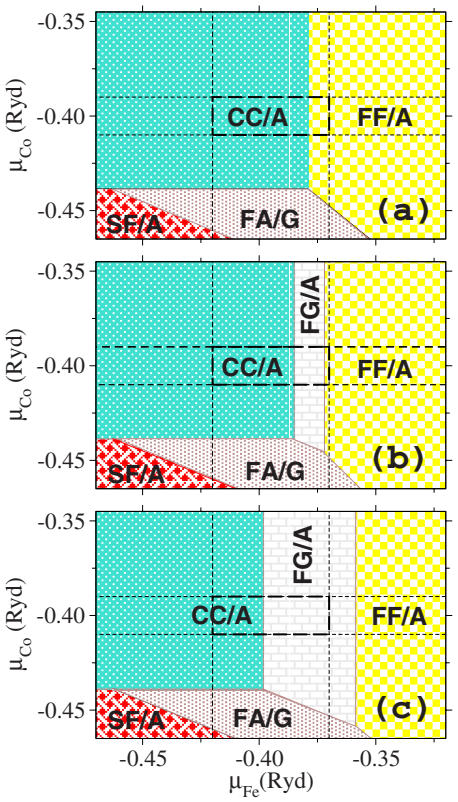

FIG. 6. (Color online) The calculated phase diagrams of the ideal and modified terminations of $Co_2FeSi/GaAs(001)$ interface at three values of As chemical potential: (a) higher limit of μ_{As} (−0.22 Ry), (b) μ_{As}=−0.26 Ry, and (c) lower limit of μ_{As} (−0.27 Ry). The shadings show the regions of stability of various terminations, thin dashed lines mark the low and high limits of the chemical potentials, and the thick dashed lines indicate the thermodynamically accessible region of the phase diagrams. The capital letters C, F, S, G, and A stand for Co, Fe, Si, Ga, and As atoms.

side and Ga and As terminations in the semiconductor side. Besides, Co_2FeSi with L21 structure may be considered as two zinc-blende sublattices: CoFe and CoSi. So, for each termination there exist two possible CoFe and CoSi patterns depending on which sublattice (CoFe or CoSi) continues the GaAs zinc-blende structure. In the case of SiFe/As and SiFe/Ga terminations, we computed both possible patterns within GGA and found out that the CoFe pattern is more favorable. In the case of CoCo/As and CoCo/Ga terminations, the difference between two possible patterns is a negligible second-order term. Therefore, for these terminations only the CoFe pattern was considered.

In addition to the four ideal terminations, we studied four modified FeFe/As, FeFe/Ga, FeGa/As, and FeAs/Ga terminations (Fig. 6). The Fe rich interfaces were considered because our surface studies confirmed the stability of the free FeFe surface. Following the same arguments presented for CoCo terminations, in the FeFe termination also only CoFe pattern was considered. Our motivation for the investigation of the modified FeAs/Ga and FeGa/As terminations was the experimental observation of mix layers at $Co_2FeSi/GaAs$ interface.[12,13] Since Si atom, similar to Ga and As atoms, has an *sp* valence shell, AsFe and GaFe layers may be the more

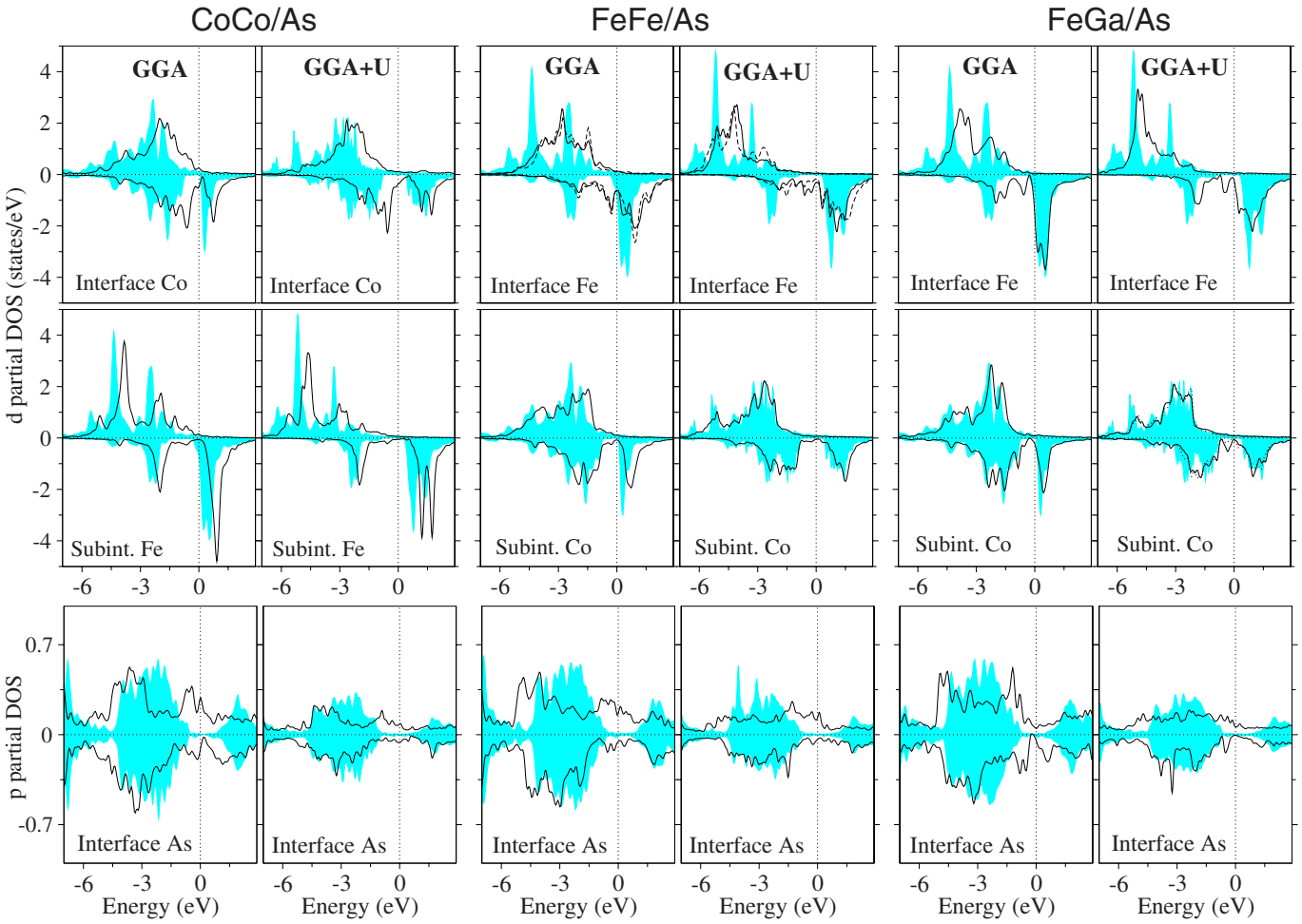

FIG. 7. (Color online) The *d* partial DOS of the interface and subinterface (Subint.) Co and Fe atoms and *p* partial DOS of the interface As atom at the stable interface terminations within GGA and GGA+*U*. The shaded areas show corresponding bulk partial DOS. The Fermi energy is set to zero.

favorable mix layers. Moreover, our test calculations show that mix Co layers are not feasible in this heterostructure.

To determine the relative stability of different possible patterns and terminations, the phase diagram of interfaces was calculated by comparing corresponding interface energies calculated again according to Eq. (1). But here because of larger number of independent atomic chemical potentials, we plotted the phase diagram for three different values of As chemical potential: the higher (−0.22 Ry) and lower (−0.27 Ry) limits of μ_{As} and also a point between these limits (−0.26 Ry). Note that the equilibrium relation $\mu_{Ga}+\mu_{As}=g_{GaAs}$ bounds μ_{As} and μ_{Ga} and hence we can substitute μ_{Ga} with $(g_{GaAs}-\mu_{As})$.

The results indicate that at high values of As chemical potential, the standard CoCo/As and modified FeFe/As terminations occupy the whole accessible region of the phase diagram and all other terminations are out of this area. By decreasing μ_{As}, the modified FeGa/As termination also appears in the stability area of the phase diagram. Therefore, one may expect that in Ga rich environments, a mixed FeGa layer may form at the interface. It is in agreement with the calculated cohesive energy of Co_2FeGa Heusler alloy (Table I) which is very close to Co_2FeSi cohesive energy, indicating low-energy cost of Si replacement with Ga atom at the interface.

We observe that the standard SiFe/As and mixed FeAs/Ga terminations are far from the allowed region, regardless of the value of the As chemical potential. The instability of the mixed FeAs/Ga interface is consistent with the higher cohesive energy of Co_2FeAs compared to Co_2FeSi alloy (Table I). Notably, not all standard Ga-terminated interfaces appear in the phase diagram, indicating the instability of these terminations compared to As-terminated interfaces.

In order to investigate the interface effects on the electronic and magnetic properties of the stable $Co_2FeSi/GaAs(001)$ interfaces, we calculated the interface atomic PDOS plotted in Fig. 7 and magnetic moments given in Table IV. Similar to the surfaces and contrary to the bulk states, all interface terminations have a rather high negative interface Fermi-level spin polarization. It is visible that almost at all terminations, the atomic PDOS of Heusler alloy moves toward higher energies, while at the semiconductor side, As *p* states shift to lower energies. These opposite shifts in two sides of the interfaces are due to the potential lineup across interfaces (will be shown). The shift of the interface Heusler atom PDOS toward higher energies destroys the half

TABLE IV. The Interface and subinterface atomic magnetic moments (μ_B) at the stable interface terminations. The interface values are bold to be more recognizable.

		FeGa/As	CoCo/As	FeFe/As
GGA	Fe	**3.12**	2.99	**2.88,2.77**
	Co	1.25,1.19	**1.17,1.04**	1.48,1.30
GGA+U	Fe	**3.19**	3.12	**3.19,3.20**
	Co	1.54,1.56	**1.52,1.39**	1.72,1.70

metallicity of the system. In addition, the density of states of the interface Co, Fe, and As are visibly more broadened than the corresponding bulk DOS, indicating strong Co-As and Fe-As interface bondings. This statement is confirmed by the interface atomic magnetic moments of the FeFe/As and CoCo/As terminations within GGA (Table IV), which are substantially lower than the bulk values. The decrease in the magnetic moments at this interface is originated from the considerable p-d hybridization in the Co-As and Fe-As interface bonds. The obtained interface magnetic moments at FeGa/As termination indicate that mixing with Ga compensates for the strong FeAs bonding at the interface and enhances the interface magnetic moments. In contrast to Co-As and Fe-As, the interface Si-As bonding is rather weak, and thus the Si p partial DOS (not shown in the figure) is not more broadened than the corresponding bulk DOS.

The data in Table IV indicate that GGA+U, similar to the free surfaces, compensate for some interface effects and enhance the reduced interface magnetic moments toward bulk values.

For more investigation of the interface bonds, the relaxed atomic positions at the stable interfaces were accurately considered and plotted in Fig. 8. It is seen that after relaxation, the interface As atoms move toward interface Co and Fe atoms in the pure Co- and Fe-terminated interfaces, indicating strong interface Fe-As and Co-As bondings. While in the mixed FeGa/As termination, the interface atoms stay almost

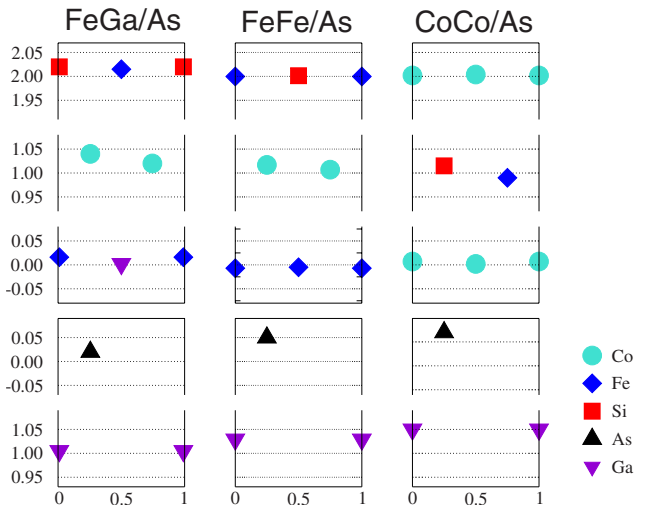

FIG. 8. (Color online) Similar to Fig. 5 but for the stable interface terminations.

in their ideal positions. It may be an evidence for longer interface Ga-As bond compared to interface Fe-As and Co-As bond lengths. It is understood as the reason behind the different behavior of the interface magnetic moments in the FeGa termination compared with the FeFe and CoCo terminations. The observation of CoAs and $Co_xFe_{(1-x)}As(0<x<3)$ alloys at $Co_2FeSi/GaAs$ interface may be an experimental evidence for strong Co-As and Fe-As bondings at this interface.[12,13]

The subinterface Co atoms in the mixed FeGa/As termination displaces slightly toward interior Heusler layers. It is another reason for increasing atomic magnetic moments at this interface and is attributed to the fact that the interface Co-Si bond is stronger than the interface Co-Ga bond. Therefore, the subinterface Co atoms in the FeGa/As termination half of whose Co-Si bonds are replaced with Co-Ga move toward the next FeSi layers.

Of important aspects of interfaces to be studied are band alignments. These quantities are relevant to control transport properties in heterojunction devices. In fact, a half-metal/semiconductor junction resembles a metal/semiconductor junction in the majority-spin channel and a semiconductor/semiconductor in the minority-spin channel. In metal/semiconductor contacts, the relevant band alignment parameters are p-type or n-type Schottky barriers defined as the difference between semiconductor valence-band (VB) maximum (VBM) or conduction-band (CB) minimum (CBM) and metal Fermi level; while in semiconductor/semiconductor contacts the valence-(conduction-)band offset is defined as the difference between valence-(conduction-)band edges in half metal and semiconductor. In practice, to achieve the band diagram of a heterojunction, one may apply potential lineup to align two independently calculated bulk band structures of two materials. But noting that within local-density approximation (LDA)/GGA calculations the band gap of GaAs is not obtained consistent with experiment, a scissors shift was applied to the conduction band of GaAs to fit the band gap with experimental value.

In order to determine the potential line-up parameter, we follow Peressi *et al.* and apply a two-step averaging scheme to the electrostatic potential at the interface.[34] First, the electrostatic potential was averaged over xy planes in the supercell to obtain the in-plane average potential. The obtained average potential for the stable CoCo/As termination, as a prototype, is plotted in Fig. 9 and represents two periodic functions joining smoothly at the interface. The periods of oscillations of these two functions are equal to half of the bulk lattice constants on both sides of the interface. The obvious offset of these two functions at the interface is the potential lineup. For more accurate determination of the potential lineup, we applied a macroscopic averaging over the periods of oscillations to obtain a rather sharp potential step function at the interface. The macroscopic average potentials at CoCo/As termination, as a prototype, are plotted in Fig. 9. In this way, we determined the electrostatic potential lineups of about 0.90, 0.88, and 0.89 Ry for CoCo/As, FeFe/As, and FeGa/As interface terminations, respectively.

We used the obtained potential lineup and bulk electronic structure to determine the band diagram of the stable terminations of $Co_2FeSi/GaAs$ junction. The obtained band align-

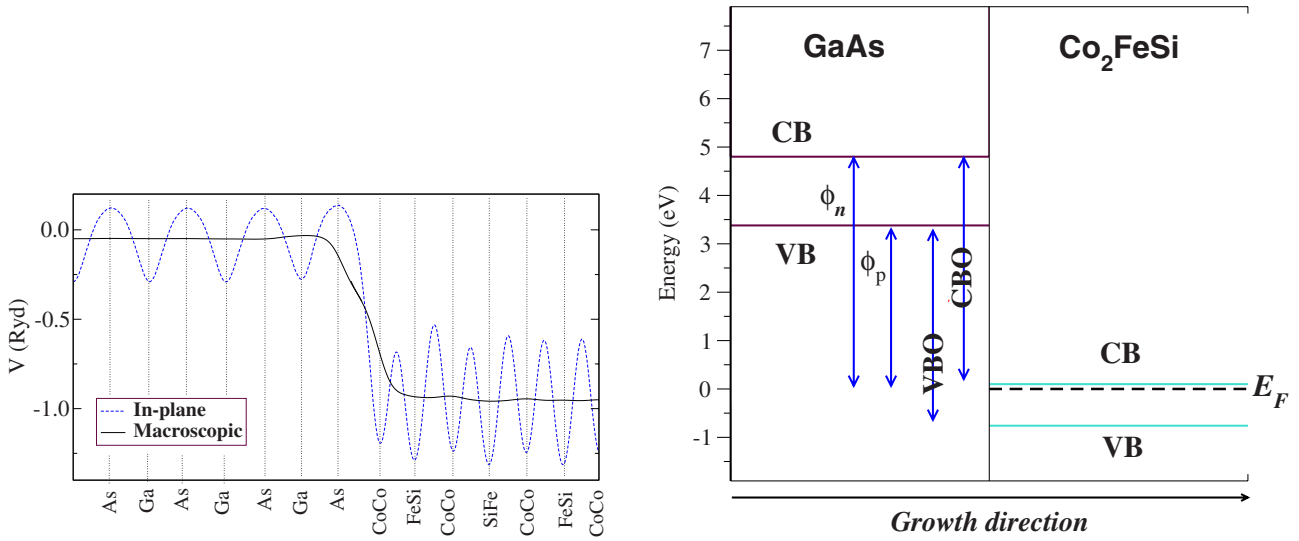

FIG. 9. (Color online) Top: the in-plane and macroscopic average potential across the CoCo/As-terminated interface. Bottom: the schematic band diagram of the CoCo/As-terminated $Co_2FeSi/GaAs(001)$ heterostructure. VB, CB, and E_F indicate the valence band, the conduction band, and the Heusler alloy Fermi energy which is set to zero.

ment parameters are reported in Table V along with the band alignment parameters of some other similar heterostructures. It is observed that $Co_2FeSi/GaAs(001)$ heterojunction has substantially larger valence- and conduction-band offsets compared with some other Heusler alloy or binary half-metal-based heterostructures. These large offsets act as obstacles for spin injection from Heusler contact into GaAs semiconductor in the spin-down channel.

It is observed that all stable terminations of this heterostructure have negative *p* Schottky barrier. It is due to the fact that the work function of the $Co_2FeSi(001)$ surface (2.91 eV) is smaller than the electron affinity of GaAs (4.07 eV). A metal/semiconductor contact with a negative Schottky barrier would behave Ohmically with a low internal resistance. Guo and Lundstrom, by solving the two-dimensional Poisson equation, showed that such contacts are promising for developing ballistic field-effect transistors.[38] Although, measuring a negative Schottky barrier is a new challenge in the semiconductor technology, there are some strong experimental evidences for the realization of this phenomena.[39–41] Tao and Zhu strongly claimed that the barrier height between Ti- and Se-passivated *n*-type Si(001) is negative or nearly negative.[41] Javey *et al.*, by using Pd contacts, succeeded to fabricate high-performance ballistic nanotube field-effect transistors with zero or slightly negative Schottky barriers.[42] Therefore, it seems that heterostructures of Co_2FeSi and *p*-type GaAs are promising junctions for spin transport applications.

VI. SUMMARY AND CONCLUSIONS

Density-functional theory calculations of the structural (within GGA), electronic, and magnetic (within GGA and GGA+*U*) properties of (001) surface of Co_2FeSi Heusler alloy and its interface with GaAs(001) were reported. Phase diagram of the surfaces shows that either the standard (CoCo and SiFe) or the modified FeFe terminations are thermodynamically realizable. It was argued that the surface Co-Si bond is considerably stronger than the surface Co-Fe bond. Although GGA+*U* is able to recover the half-metallic behavior of bulk Co_2FeSi, we observed that within both GGA and GGA+*U* some surface states substantially reduce the Fermi-level spin polarization of the $Co_2FeSi(001)$ surfaces to some negative values.

TABLE V. The band alignment parameters (in eV) of the stable terminations of $Co_2FeSi/GaAs(001)$ heterojunction (top panel) and some other half-metal/semiconductor junctions given for comparison (bottom panel). TW stands for this work.

Heterostructure	ϕ_n	ϕ_p	VBO	CBO	Ref.
CoCo/As	4.84	−3.42	3.52	4.76	TW
FeFe/As	4.54	−3.12	3.22	4.46	TW
FeGa/As	4.67	−3.23	3.33	4.59	TW
$Co_2Cr_{0.5}Fe_{0.5}Al/GaAs$	2.20	−0.78	0.32	1.93	21
$Co_2MnSi/GaAs$	1.20	0.18	0.03	0.50	35
NiMnSb/GaAs	0.32	1.13	0.62	0.32	36
CrSe/ZnSe	1.84	0.88	1.94	1.28	37

The obtained phase diagram for $Co_2FeSi/GaAs(001)$ interface shows that the ideal SiFe interface terminations are not achievable, while CoCo/As termination occupies the major part of the accessible region of the phase diagram. The results indicate that in addition to the ideal CoCo/As termination, some modified interface terminations may also form in limited parts of the allowed region. The modified FeFe/As termination could be stabilized close to the high μ_{Fe} and μ_{As} limits, while increasing the Ga chemical potential favors the formation of the mixed FeGa/As interface. Inspecting the relaxed interface atomic positions clarifies the visible tendency of As to make strong bonds with transition atoms at the pure Fe and Co interface terminations. Similar to the surface results, some interface states destroy the half-metallic behavior of $Co_2FeSi/GaAs(001)$ interfaces within both GGA and GGA+U and result in a large negative interface spin polarization. Calculating the band alignment parameters resulted in large negative p-type Schottky barriers in all stable terminations of this heterostructure.

ACKNOWLEDGMENTS

This work was jointly supported by the Vice Chancellor for Research Affairs of Isfahan University of Technology, Centre of Excellence for Environmental Nanotechnology, and ICTP Affiliated Centre.

[1] J. M. D. Coey, M. Venkatesan, and M. A. Bari, *Lecture Notes in Physics* Vol. 595, edited by C. Berthier, L. P. Levy, and G. Martinez (Springer, New York, 2002).
[2] G. Schmidt, D. Ferrand, L. W. Molenkamp, A. T. Filip, and B. J. van Wees, Phys. Rev. B **62**, R4790 (2000).
[3] S. Picozzi, A. Continenza, and A. J. Freeman, Phys. Rev. B **69**, 094423 (2004).
[4] L. J. Singh, Z. H. Barber, Y. Miyoshi, W. R. Branford, and L. F. Cohen, J. Appl. Phys. **95**, 7231 (2004).
[5] S. Kämmerer, A. Thomas, A. Hütten, and G. Reiss, Appl. Phys. Lett. **85**, 79 (2004).
[6] K. H. J. Buschow, P. G. V. Engen, and R. Jongebreur, J. Magn. Magn. Mater. **38**, 1 (1983).
[7] S. Wurmehl, G. H. Fecher, H. C. Kandpal, V. Ksenofontov, C. Felser, H.-J. Lin, and J. Morais, Phys. Rev. B **72**, 184434 (2005).
[8] S. Wurmehl, G. H. Fecher, H. C. Kandpal, V. Ksenofontov, C. Felser, and H. J. Lin, Appl. Phys. Lett. **88**, 032503 (2006).
[9] J. Hamrle *et al.*, J. Phys. D **40**, 1558 (2007).
[10] J. Hamrle, S. Blomeier, O. Gaier, B. Hillebrands, H. Schneider, G. Jakob, K. Postava, and C. Felser, J. Phys. D **40**, 1563 (2007).
[11] H. C. Kandpal, G. H. Fecher, C. Felser, and G. Schonhense, Phys. Rev. B **73**, 094422 (2006).
[12] M. Hashimoto, J. Herfort, A. Trampert, H. P. Schönherr, and K. H. Ploog, J. Vac. Sci. Technol. B **24**, 2004 (2006).
[13] M. Hashimoto, J. Herfort, H. P. Schönherr, and K. H. Ploog, J. Appl. Phys. **98**, 104902 (2005).
[14] Z. Gercsi, A. Rajanikanth, Y. K. Takahashi, K. Hono, M. Kikuchi, N. Tezuka, and K. Inomata, Appl. Phys. Lett. **89**, 082512 (2006).
[15] K. Inomata, N. Ikeda, N. Tezuka, R. Goto, S. Sugimoto, M. Wojcik, and E. Jedryka, Sci. Technol. Adv. Mater. **9**, 014101 (2008).
[16] V. Niculescu, J. I. Budnick, W. A. Hines, K. Raj, S. Pickart, and S. Skalski, Phys. Rev. B **19**, 452 (1979).
[17] S. J. Hashemifar, P. Kratzer, and M. Scheffler, Phys. Rev. Lett. **94**, 096402 (2005).
[18] M. Zhang, A. L. Wolf, L. Zhang, O. Tegus, E. Bruck, G. Wu, and F. R. de Boer, J. Appl. Phys. **97**, 10C301 (2005).
[19] H. J. Elmers *et al.*, Phys. Rev. B **67**, 104412 (2003).
[20] G. Jakob, F. Casper, V. Beaumont, S. Falk, N. Auth, H.-J. Elmers, C. Felser, and H. Adrian, J. Magn. Magn. Mater. **290-291**, 1104 (2005).
[21] S. Zarei, S. J. Hashemifar, H. Akbarzadeh, and Z. Haffari, J. Phys.: Condens. Matter **21**, 055002 (2009).
[22] M. P. Raphael, B. Ravel, Q. Huang, M. A. Willard, S. F. Cheng, B. N. Das, R. M. Stroud, K. M. Bussmann, J. H. Claassen, and V. G. Harris, Phys. Rev. B **66**, 104429 (2002).
[23] P. Brown, K. Neumann, P. Webster, and K. Ziebeck, J. Phys.: Condens. Matter **12**, 1827 (2000).
[24] K. H. J. Buschow and P. G. van Engen, J. Magn. Magn. Mater. **25**, 90 (1981).
[25] A. Deb, M. Itou, Y. Sakurai, N. Hiraoka, and N. Sakai, Phys. Rev. B **63**, 064409 (2001).
[26] R. Y. Umetsu, K. Kobayashi, A. Fujita, K. Oikawa, R. Kainuma, K. Ishida, N. Endo, K. Fukamichi, and A. Sakuma, Phys. Rev. B **72**, 214412 (2005).
[27] J. P. Perdew, K. Burke, and M. Ernzerhof, Phys. Rev. Lett. **77**, 3865 (1996).
[28] M. Methfessel and A. T. Paxton, Phys. Rev. B **40**, 3616 (1989).
[29] H. J. Monkhorst and J. D. Pack, Phys. Rev. B **13**, 5188 (1976).
[30] T. Bandyopadhyay and D. D. Sarma, Phys. Rev. B **39**, 3517 (1989).
[31] I. Galanakis, P. H. Dederichs, and N. Papanikolaou, Phys. Rev. B **66**, 174429 (2002).
[32] K. Reuter, C. Stampfl, and M. Scheffler, in *Handbook of Materials Modeling*, edited by S. Yip (Kluwer, Dordrecht, 2004), and references therein; http://www.fhi-berlin.mpg.de/th/pub04.html
[33] K. Reuter and M. Scheffler, Phys. Rev. B **65**, 035406 (2001).
[34] M. Peressi, N. Binggeli, and A. Baldereschi, J. Phys. D **31**, 1273 (1998).
[35] N. Ghaderi, S. J. Hashemifar, H. Akbarzadeh, and M. Peressi, J. Appl. Phys. **102**, 074306 (2007).
[36] A. Debernardi, M. Peressi, and A. Baldereschi, Comput. Mater. Sci. **33**, 263 (2005).
[37] E. Hazrati, S. J. Hashemifar, and H. Akbarzadeh, J. Appl. Phys. **104**, 113719 (2008).
[38] J. Guo and M. S. Lundstrom, IEEE Trans. Electron Devices **49**, 1897 (2002).
[39] M. Tao, D. Udeshi, S. Agarwal, E. Maldonado, and W. P. Kirk, Solid-State Electron. **48**, 335 (2004).
[40] J. Osvald, Solid-State Electron. **48**, 2347 (2004).
[41] M. Tao and J. Zhu, Solid-State Electron. **48**, 2351 (2004).
[42] A. Javey, J. Guo, Q. Wang, M. Lundstrom, and H. Dai, Nature (London) **424**, 654 (2003).